Electrochemical and Solid-State Letters, **8** (3) G78-G81 (2005)
1099-0062/2005/8(3)/G78/4/$7.00 © The Electrochemical Society, Inc.

Minority Carrier Lifetime Properties of Reactive Ion Etched p-Type Float Zone Si

Prakash N. K. Deenapanray,[a,z] M. Hörteis,[b,d] Daniel Macdonald,[c] and K. J. Weber[a]

[a]*Department of Engineering, Centre for Sustainable Energy Systems, The Australian National University, Canberra ACT 0200, Australia*
[b]*Department of Electronic Materials Engineering, Research School of Physical Sciences and Engineering, The Australian National University, Canberra ACT 0200, Australia*
[c]*Department of Engineering, The Australian National University, Canberra ACT 0200, Australia*

Quasi-steady-state photoconductance (QSSPC) and deep level transient spectroscopy (DLTS) were used to characterize the minority carrier lifetime properties of reactive ion etched p-type Si. The effective lifetime of the plasma-processed samples degraded after etching, with the densities of recombination centers increasing linearly with etch time. Evidence is provided for the long-range ($>2\ \mu m$) migration of defects in the plasma-etched samples. A discrete defect with energy position at (0.32 ± 0.02) eV, that could be either B- or H-related, was detected by DLTS in the etched samples. Furthermore, this energy level could be used to adequately model the injection-dependence of the measured carrier lifetimes using the Shockley-Read-Hall model. Our results show that DLTS and QSSPC is a powerful combination to characterize the electrical properties of defects that are relevant to the performance of solar cells.
 [DOI: 10.1149/1.1854116]

Manuscript submitted October 7, 2004; revised manuscript received November 2, 2004. Available electronically January 24, 2005.

Plasma (or dry) etching has become a dominant technique in semiconductor processing because it provides highly anisotropic etch profiles with good selectivity.[1,2] Etching of vias and trenches in SiO_2 is now a critical step in the fabrication of multilevel interconnects for the ultralarge scale integration of Si devices.[3] Further, nanometer-size patterns are routinely patterned onto polysilicon, SiO_2 or Si_3N_4 using plasma etching for fabricating devices and structures as diverse as semiconductor memories,[4,5] photonic crystals,[6,7] high electron mobility transistors,[8] laser diodes,[2] and microelectromechanical systems.[9] There are, however, areas of semiconductor research where plasma etching has not made a significant impact. In the field of photovoltaics (PV), the fabrication of silicon solar cells is still heavily reliant on wet chemical etching. Previous studies have used plasma etching in silicon solar cell processing either as a substitute for all wet chemistry[10] or for a specialized purpose, such as metallization.[11] However, plasma etching creates defects in the near-surface region of the exposed semiconductor.[12-14] The electrical properties of the solar cells usually degrade in the presence of electrically active defects that may act as either trapping or recombination centres.[15] Schaefer and Ludeman have reported a nearly damage-free RIE process for solar cell processing, whereby dry processed solar cells show the same performance as wet etched cells.[14]

The need to increase the price competitiveness of PV relative to nonrenewable energy sources calls for new concepts in solar cell design and fabrication. In this respect, a novel low-cost, high-efficiency micromachined Si solar cell has recently been developed at the Australian National University.[16] The innovative features of the new cells include the improved Si utilization by a factor ~12, a reduction in the number of wafers per kW by ~30, high efficiency and perfect bifacial response. Reactive ion etching (RIE), in conjunction with wet chemistry, is one option that can be used in the micromachining and metallization steps of the new technology. The number of steps in our process could be reduced by elimination of a few chemical etch steps by etching SiO_2 and/or Si_3N_4 layers through to the Si substrate. This is desirable for reducing device fabrication complexity, and to minimize the use of toxic hydrofluoric acid. To judge the desirability of etching through to the Si substrate, intimate knowledge about the electrical properties of plasma-etched Si is required. In this paper, we investigate the influence of reactive ion etching in a CHF_3/O_2 plasma on the minority carrier lifetime of p-type float zone Si. We also demonstrate that deep level transient spectroscopy and minority lifetime measurements as used here is a powerful combination for characterizing the electrical properties of defects that adversely influence the performance of solar cell materials.

Experimental

Two 4 in. boron-doped float zone (FZ) wafers labeled A and B with resistivity 0.75-1.25 and 140-150 Ω cm, respectively, were used. The wafers were polished in a $HF:HNO_3$ (1:12 by volume) mixture prior to RIE in an Oxford PlasmaLab80 system. After chemical polishing, the wafers were between 480 and 500 μm thick, and they were cleaved into quarters for plasma etching. Samples from B were exposed to a CHF_3/O_2 plasma for 30 s to 5 min, while samples from wafers A were exposed for 5 min. The CHF_3/O_2 plasma has a high etch selectivity for Si_3N_4 or SiO_2 over photoresist and Si.[17] In this study, RIE was performed at 23°C in a mixture of 50 sccm CHF_3 and 5 sccm O_2 at a process pressure of 55 mTorr. In our RIE system, the samples are placed on a water-cooled electrode that it maintained at 23°C by a water chiller. The rf power was 200 W, yielding a dc self-bias in the range 450-500 V. These parameters were chosen based on the processing that we typically use in the fabrication of our novel thin-film Si solar cells.[16] After RIE, the samples were chemically cleaned prior to light phosphorous diffusion and oxidation. This high temperature step serves two purposes, namely, it mimics the post-RIE high temperature processing in our solar cell fabrication scheme, and it provides surface passivation for minority carrier lifetime measurements. The surface passivation of samples was completed with a forming gas anneal at 400°C.[18] Control samples (*i.e.*, no RIE) of each resistivity were subject to identical etching, cleaning and surface passivation steps as the plasma-treated samples. The control samples allow the recombination rate due to all processes other than those caused by RIE, such as recombination at the surfaces, and recombination in the bulk due to Auger recombination and potential contamination arising from the annealing, etching and cleaning steps, to be measured. To determine the depth of Si surface modification due to RIE, selected samples from wafer B were chemically etched for times between 15 s and 2 min prior to surface passivation.

The minority carrier lifetime of samples was determined using the quasi-steady-state photoconductance method (QSSPC),[19] which measures lifetime as a function of excess carrier density Δn. Hence,

[d] Present address: Lehrstuhl für Experimentalphysik IV, Institu für Physik, Universität Augsburg, 86135 Augsburg, Germany.
[z] E-mail: prakash.deenapanray@anu.edu.au

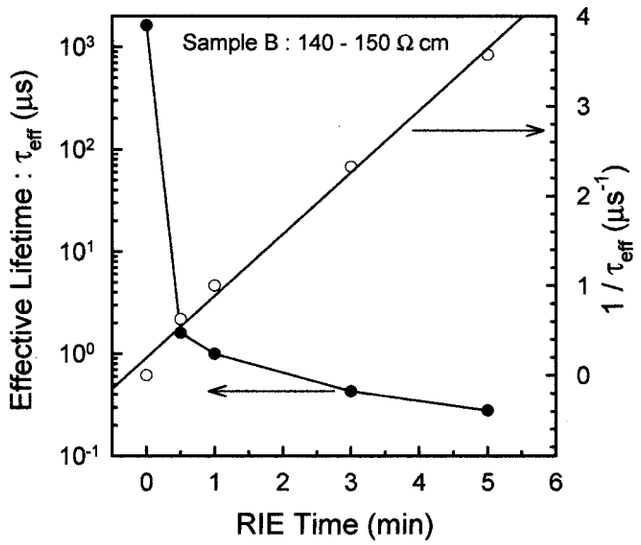

Figure 1. Variations of τ_{eff} (solid circles) and $1/\tau_{eff}$ (open circles) as a function of etch time.

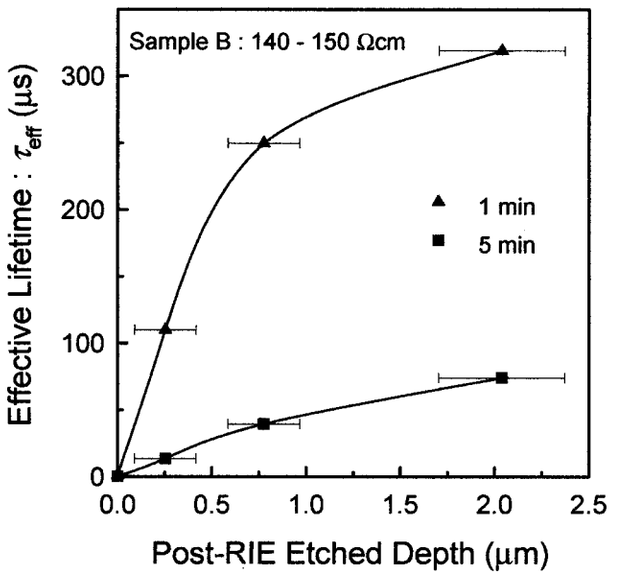

Figure 2. Variation of effective lifetime as a function of the amount of Si surface etched back after RIE. RIE was carried out on sample B for either 1 or 5 minutes.

lifetime comparisons between wafers at the same value of Δn can be made, which, depending on the magnitude of the lifetime, may not correspond to the same illumination intensity. The measured quantity is known as an effective lifetime, τ_{eff}, and incorporates the impact of recombination both in the bulk and at the surfaces. Deep level transient spectroscopy (DLTS) was performed on the control and plasma-etched samples from wafer A using a modified lock-in-type setup. We chose wafer A for DLTS measurements because of its lower resistivity. In this case, the lower zero-bias depletion layer was small (~0.32 μm compared to ~3.5 μm for wafer B), that allowed us to probe defects close to the surface where they are produced during RIE. Prior to metallisation, the phosphorous-diffused layer of samples was chemically etched. Schottky diodes were fabricated on samples by thermal evaporation of Ti (~75 nm thick and 0.5 mm diam) through a metal contact mask. Selected samples were annealed under Ar for 15 min between 120 and 230°C to study the thermal stability of defects.

Results and Discussion

Figure 1 shows the effective lifetime, τ_{eff}, at an excess carrier density of $\Delta n = 1 \times 10^{14}$ cm^{-3} of wafer B as a function of RIE time. Results are shown for sample B because the effect of time was more clearly resolved for this set of sample because of the high initial effective lifetime. An etch time as short as 30 s reduced τ_{eff} by three orders of magnitude showing the pronounced detrimental effect of RIE on the minority carrier lifetime. The results can be better analyzed by looking at the inverse of the effective lifetime, $1/\tau_{eff}$. Based on the Shockley-Read-Hall(SRH) theory of carrier generation and recombination at a discrete defect level in p-Si, the SRH lifetime can be expressed as[20,21]

$$\frac{1}{\tau_{SRH}} = \frac{N_A + \Delta n}{\tau_{p0}(n_1 + \Delta n) + \tau_{n0}(N_A + p_1 + \Delta n)} \quad [1]$$

where, $\Delta n = \Delta_p$ is the excess carrier density. The capture time constants τ_{n0} and τ_{p0} are related to the thermal velocity (ν_{th}), the recombination center density (N_t), and capture cross section (σ) via $\tau_{n0} = 1/(\nu_{th}\sigma_n N_t)$ and $\tau_{p0} = 1/(\nu_{th}\sigma_p N_t)$. It becomes clear from Eq. 1 that $1/\tau_{SRH}$ is proportional to the density of the recombination center, N_t. Because the minority carrier lifetime in our plasma-etched sample is at least three orders of magnitude lower than in the control sample, the effective lifetime that we measure corresponds to the SRH recombination in the bulk of an etched sample. Hence, reading from the right axis of Fig. 1 shows that the density of recombination centers in plasma-etched samples increased linearly with etch time. Following RIE, and prior to surface passivation, selected samples were dipped in a mixture of HF/HNO_3 for different times to etch controlled thicknesses of the plasma exposed surface layers. The results are shown in Fig. 2 for 1 min or 5 min plasma-etched sample B. The data points for the zero post-RIE etched depth correspond to the data points for 1 or 5 min RIE time in Fig. 1. Note that the room temperature chemical etching of Si exhibited fairly large variances as depicted by the horizontal error bars. The results in Fig. 2 show that τ_{eff} could be recovered by the successive removal of the damaged surfaces. However, this recovery is only partial, as the curves in Fig. 2 tend to level-off with the increasing etch depth. This clearly shows that defects generated in the near-surface region of the samples exposed to the plasma diffused to depths exceeding 2 μm even before the high-temperature steps.

QSSPC provides valuable information regarding the extent of recombination, but it does not provide any information regarding the specific electrical parameters of the recombination centers. For the latter, we have used DLTS measurements. Figure 3 shows DLTS spectra taken from control (solid triangles) and plasma-etched (open symbols) low-resistivity samples (*i.e.*, A). The control sample contained a defect A (0.54 eV) which has an energy position, $E_t = (0.54 \pm 0.02)$ eV, above the valence band edge, and apparent capture cross section, $\sigma_a \approx 8.5 \times 10^{-14}$ cm^2. RIE introduced another defect B(0.32 eV), with $E_t = (0.32 \pm 0.02)$ eV above the valence band edge and $\sigma_a \approx 4.2 \times 10^{-14}$ cm^2. The "signatures" (*i.e.*, E_t and σ_a) of defects were determined from the Arrhenius plots of $\ln(T^2/e_h)$ *vs.* $1000/T$, where e_h is the hole emission rate and T is the measurement temperature, shown in Fig. 4a.

In Fig. 4a, the experimental data points are shown in open symbols, while the solid symbols correspond to the "signatures" of defects H(0.52) and H(0.33) that were reconstructed from data reported in the literature.[22] A recent study has shown that H(0.52) was at least constituted from a B_i-H pair, and that it was most likely to be the B_i-B_s-H complex. Isochronal annealing experiments of H(0.52)[22] and a similar defect H(0.56)[23] revealed that the concentration of this defect increased within the range of 100 to 150°C, followed by a sharp decrease at higher temperatures. The isochronal annealing results shown in Fig. 4b reveal the similar annealing behavior of A (0.54 eV). Based on the results shown in Fig. 4, we

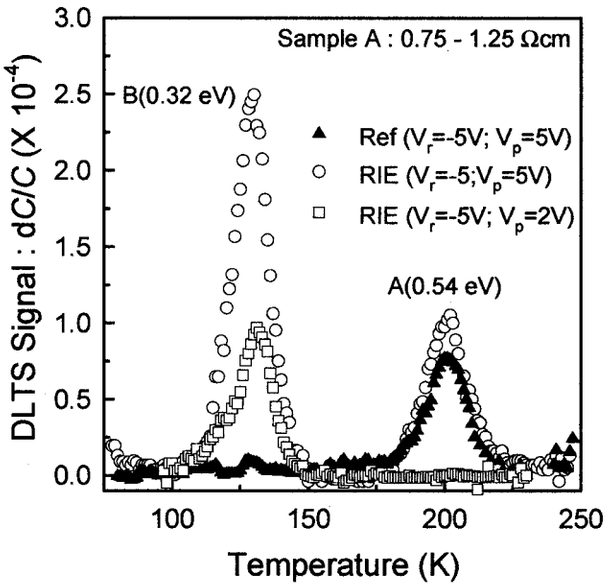

Figure 3. DLTS spectra taken from control (solid triangles) and reactive ion etched (open symbols) sample A. The sample had a ~2 μm thick surface layer etched back after RIE. The bias conditions were such that the region extending between ~0.32 and ~0.65 μm was probed for the spectrum shown in open squares, whereas the region probed was between ~0.32 and ~0.9 μm for the spectrum in open circles.

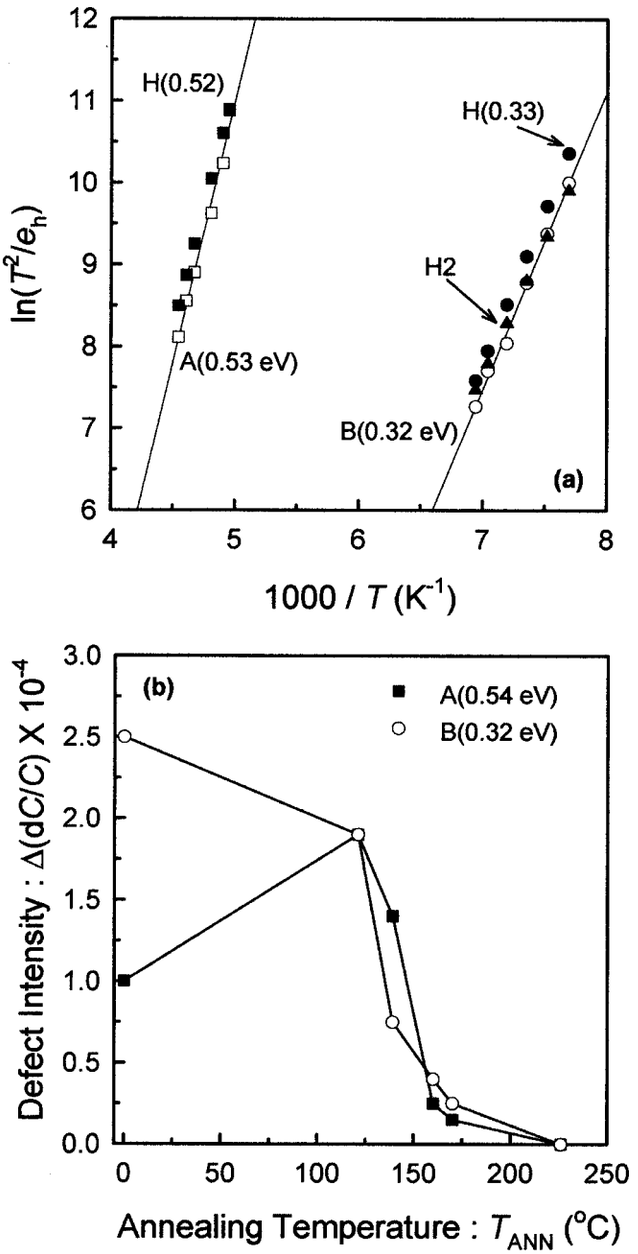

Figure 4. (a) Arrhenius plots from which the "signatures" of defects were determined. The data shown in solid symbols show the "signatures" of hole traps previously reported in the literature. (b) isochronal annealing behavior of A (0.54 eV) and B (0.32 eV).

suggest that A (0.54 eV) is probably the B_i-B_s-H complex. A comparison between the DLTS spectra shown in open circles and open triangles in Fig. 3, reveals that A (0.54 eV) was confined within approximately the top 0.6 μm of the plasma-etched sample. This probably reflects the in-diffusion of hydrogen during chemical etching in HF solution.

As can be seen from Fig. 4a, the "signature" of B (0.32 eV) is similar to that of H2[24] (solid triangles) and H(0.33) (solid circles).[22] H2 is similar to defect H(148 K),[25] that has been reported in proton-implanted Cz and FZ Si, respectively. Furthermore, the two defects have been shown to be H-related hole traps. Because H is present in our samples [A (0.54 eV) is H-related] and the "signature" of B (0.32 eV) is similar to H2 and H (148 K), it is tempting to conclude that B (0.32 eV) is probably H-related. However, B (0.32 eV) has a lower thermal stability that both H2 and H (148 K). B (0.32 eV) is unstable above 125°C, whereas H (148 K) and H2 are stable up to 300 and 250°C, respectively. On the other hand, H (0.33), that has been proposed to be B-related,[22] has a similar annealing behavior as B (0.32 eV). Furthermore, a defect H1 with similar electronic and annealing properties as B (0.32 eV) has previously been observed in ion implanted or electron irradiated p-type epitaxial Si.[26] H1 could not be detected in p-type samples containing a high concentration of O (*i.e.*, p-type Cz Si). It was, therefore, concluded that the H1 was a B-related defect. Because the concentration of O in FZ samples can be expected to be relatively low, our results suggest that A (0.32 eV) could be a B-related, similar to H (0.33)[22] and H1.[26] The formation of A (0.32 eV) is initiated through the formation of Si interstitials, Si_i, during the low-energy bombardment of the surface during plasma etching. These interstitials preferentially form B_i by the Watkins replacement mechanism because of the low concentrations of competing traps like C and O in FZ Si.[27] The boron interstitials then interact with other impurities to form A (0.32 eV). It is worth noting here that defect H2 in Ref. 24, that has been attributed to B, also has similar electronic and annealing properties as A (0.54 eV). H (0.33),[22] and hence A (0.32 eV), is expected to have an exponentially decaying distribution when formed at the surface, which is consistent with the results shown in Fig. 2.

We now attempt to use the electronic properties of B (0.32 eV) to model the injection dependent minority carrier lifetime measurements (selected samples only). The open symbols in Fig. 5 are the experimental data points, while the lines are fits to Eq. 1. The so-called SRH densities n_1 and p_1 in Eq. 1 are given by

$$n_1 = N_C \exp\left(-\frac{E_C - E_t}{kT}\right), \quad p_1 = N_V \exp\left(-\frac{E_t - E_V}{kT}\right) \quad [2]$$

where E_t is the energy position of the recombination center, E_C and E_V are the energies of the conduction and valence band edge, and N_C and N_V are the effective densities of states in the conduction and the valence band, respectively. When $E_F = E_t$, the n_1 and p_1 equal the equilibrium densities of electrons and holes, respectively. Be-

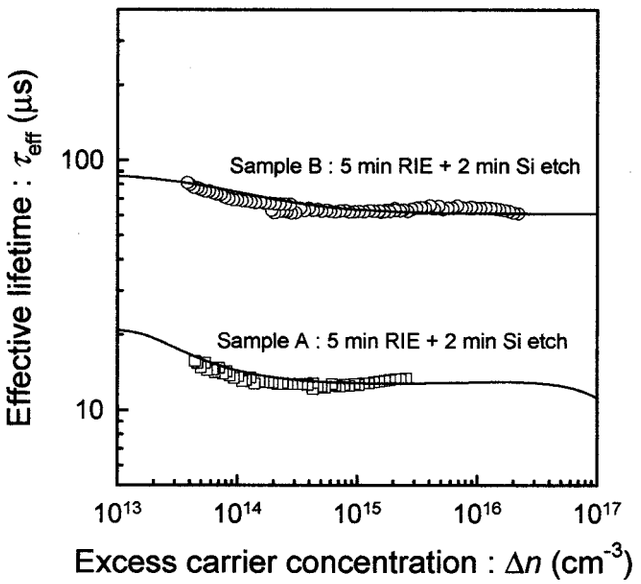

Figure 5. Modeling of the injection dependence of the minority carrier lifetimes in plasma-etched samples A and B using the SRH formalism. The solid line for sample A includes the effect of minority carrier trapping centers. The downward curvature of the model at high injection is caused by Auger recombination.

cause our DLTS measurements did not provide information regarding the capture cross section for electrons nor the effect of temperature on the majority carrier capture cross section of B (0.32 eV), we have used the room temperature values of minority and majority carrier capture cross sections for H (148 K) in Ref. 25. However, we have used the value of E_t extracted from Fig. 4a. Auger recombination was included in the modelling procedure, which impacts at high excess carrier densities.[28]

The simulations provide reasonable fits to the experimental data as shown in Fig. 5 for $N_t = 5 \times 10^{13}$ cm^{-3} (sample B) and $N_t = 2.4 \times 10^{14}$ cm^{-3} (sample A). However, the values of N_t are 5-10 times larger than what can be estimated from the DLTS data in Fig. 3. We have found that N_t became comparable to the DLTS estimate when larger values (by a factor of 10) of carrier capture cross sections were used. This highlights the uncertainty in the capture cross section values. Another point to note is that the experimental data for sample A exhibits an increase at low carrier injection that cannot be explained by the SRH formalism. This phenomenon can, however, be explained by the presence of centers which only trap and release minority carriers.[29] The effect of such minority carrier traps has been simulated in parallel with the recombination process in Fig. 5, and results in a reasonable fit to the experimental data. However, we cannot account for the presence of such trapping centers in sample A only. It should be emphasised that other combinations of energy levels and capture cross sections could also provide reasonable fits to the data, and as such we can not definitely conclude that the parameters used are correct. Nevertheless, the results at least show that an energy level of 0.32 eV is not inconsistent with the measured injection dependence. We therefore speculate that B (0.32 eV) is responsible for minority carrier lifetime degradations in our plasma-processed samples.

Finally, we would like to make a comment regarding the results in Ref. 14 that showed no significant difference between the properties of chemically- and plasma-processed solar cells. Plasma etching consists of two competing processes regarding the creation of defects, namely low-energy ion bombardment of the surface and removal of the damaged layer by a combination of physical and chemical etching. The accumulation of damage in the near-surface region of the plasma processed sample depends critically on the rate at which the damaged layer is removed. In Ref. 14, a SF_6 plasma that provides a high etch rate of Si was utilized because there was no need for a high selectivity between SiO_2 (or Si_3N_4) and Si. In our solar cell fabrication procedure,[16] we require a high selectivity between the dielectric and Si, so that the Si etch rate is very low. Another difference is the use of a higher rf power yielding a dc bias between 450 and 500 V in the present study as opposed to 100 W power producing a self-bias of only 15 V in Ref. 14.

Conclusion

In summary, we have used the combination of QSSPC and DLTS to characterize the minority carrier lifetime properties of reactive ion etched FZ p-Si. Compared to the control sample, plasma-etching degraded the lifetime of minority carrier by three orders of magnitude. A hole trap B (0.32 eV above the valence band) was detected in the etched sample, which could be either B- or H-related. We have shown that this energy level can be used to model the injection dependent minority carrier lifetime in the plasma-etched samples, although the values of the capture cross sections are uncertain. Our results have shown that QSSCC and DLTS form a powerful combination of analytical techniques for the characterization of defects that are relevant for the performance of solar cells.

Acknowledgments

The financial support of the Australian Research Council is kindly acknowledged.

The Australian National University assisted in meeting the publication costs of this article.

References

1. S. J. Fonash, *Solid State Technol.*, **28**, 150 (1985).
2. S. J. Pearton, J. C. Zopler, R. J. Shul, and F. Ren, *J. Appl. Phys.*, **86**, 1 (1999).
3. T. E. F. M. Standaert, C. Hedlund, E. A. Joseph, G. S. Oehrlein, and T. J. Dalton, *J. Vac. Sci. Technol. A*, **22**, 53 (2004).
4. Y. S. Song and C. W. Chung, *Electrochem. Solid-State Lett.*, **7**, G5 (2004).
5. S. Panda, R. Ranade, and G. S. Mathad, *J. Electrochem. Soc.*, **150**, G612 (2003).
6. M. Mulot, S. Anand, R. Ferrini, B. Wild, R. Houdre, J. Moosburger, and A. Forchel, *J. Vac. Sci. Technol. B*, **22**, 707 (2004).
7. J.-M. Lee, S. H. Oh, C.-W. Lee, H. Ko, S. Park, K. S. Kim, and M.-H. Park, *Electrochem. Solid-State Lett.*, **7**, G11 (2004).
8. W. T. Lim, I. G. Baek, P. G. Jung, J. W. Lee, G. S. Cho, J. I. Lee, K. S. Cho, and S. J. Pearton, *J. Electrochem. Soc.*, **151**, G163 (2004).
9. B. Morgan, C. M. Waits, J. Krizmanic, and R. Ghodssi, *J. Microelectromech. Syst.*, **13**, 113 (2004).
10. V. Gazuz, K. Feldrapp, R. Auer, R. Brendel, and M. Schulz, *Sol. Energy Mater. Sol. Cells*, **72**, 277 (2002).
11. S. Schaefer, R. Ludemann, and S. W. Glunz, *Prog. Photovolt: Res. Appl.*, **7**, 387 (1999).
12. C. E. Gonzalez, S. C. Sharma, N. Hozhabri, D. Z. Chi, and S. Ashok, *Appl. Phys. A: Mater. Sci. Process.*, **68**, 643 (1999).
13. O. O. Awadelkarim, P. I. Mikulan, T. Gu, K. A. Reinhardt, and Y. D. Chan, *J. Appl. Phys.*, **76**, 2270 (1994).
14. S. Schaefer and R. Ludeman, *J. Vac. Sci. Technol. A*, **17**, 749 (1999).
15. M. A. Green, in *Solar Cells-Operating Principles, Technology and System Applications*, p. 40, The University of New South Wales, Kensington (1992).
16. K. J. Weber, A. W. Blakers, M. J. Stocks, J. H. Babaei, V. A. Everett, A. J. Neuendorf, and P. J. Verlinden, *IEEE Electron Device Lett.*, **25**, 37 (2004).
17. S. K. Ray, C. K. Maiti, and N. B. Chakraborti, *Semicond. Sci. Technol.*, **8**, 599 (1993).
18. A. Cuevas, *Sol. Energy Mater. Sol. Cells*, **57**, 277 (1999).
19. R. A. Sinton and A. Cuevas, *Appl. Phys. Lett.*, **69**, 2510 (1996).
20. W. Shockley and W. T. Read, *Phys. Rev.*, **87**, 835 (1952).
21. R. N. Hall, *Phys. Rev.*, **87**, 387 (1952).
22. F. Volpi, A. R. Peaker, I. Berbezier, and A. Ronda, *J. Appl. Phys.*, **95**, 4752 (2004).
23. M. H. Yuan, D. C. Peng, Q. Z. Peng, Y. H. Zhang, J. Q. Li, and G. G. Qin, *J. Appl. Phys.*, **71**, 1182 (1992).
24. K. Irmscher, H. Klose, and K. Maass, *J. Phys. C*, **17**, 6317 (1984).
25. M. C. Huppi, *J. Appl. Phys.*, **68**, 2702 (1990).
26. S. Libertino, J. L. Benton, D. C. Jacobson, D. J. Eaglesham, J. M. Poate, S. Coffa, P. G. Fuochi, and M. Lavalle, *Appl. Phys. Lett.*, **70**, 3002 (1997).
27. G. D. Watkins, *Phys. Rev. B*, **12**, 5824 (1975).
28. M. J. Kerr and A. Cuevas, *J. Appl. Phys.*, **91**, 2473 (2002).
29. D. Macdonald and A. Cuevas, *Appl. Phys. Lett.*, **74**, 1710 (1999).